

Simulating temporal evolution of pressure in two-phase flow in porous media

Eyvind Aker*, Knut Jørgen Måløy

Department of Physics, University of Oslo, N-0316 Oslo, Norway

Alex Hansen†

Department of Physics, Norwegian University of Science and Technology, N-7034 Trondheim, Norway

(August 27, 2018)

We have simulated the temporal evolution of pressure due to capillary and viscous forces in two-phase drainage in porous media. We analyze our result in light of macroscopic flow equations for two-phase flow. We also investigate the effect of the trapped clusters on the pressure evolution and on the effective permeability of the system. We find that the capillary forces play an important role during the displacements for both fast and slow injection rates and both when the invading fluid is more or less viscous than the defending fluid. The simulations are based on a network simulator modeling two-phase drainage displacements on a two-dimensional lattice of tubes.

47.55.Mh, 07.05.Tp, 05.40.+j

I. INTRODUCTION

Fluid flow in porous media such as sand, soil and fractured rock is an important process in nature and has a huge number of practical applications in engineering. Most often mentioned is oil recovery and hydrology. Fluid flow in porous media has also been of great interest in modern physics. In particular, the different structures of the interface between the fluids in two-phase displacements have been extensively studied. Despite this attention there are still many open questions concerning fluid flow in porous media.

In this paper we report on simulations of the temporal evolution of pressure during two-phase drainage in a model porous medium, consisting of a two-dimensional lattice of tubes. The network model has been developed to measure the time dependence of different physical properties and to study the dynamics of the fluid movements. Especially, we focus on the dynamics of the temporal evolution of the pressure due to capillary and viscous forces and the time dependence of the front between the two liquids. The discussion is restricted to drainage displacement, i.e. the process where a non-wetting fluid displaces a wetting fluid in a porous medium.

During the last two decades an interplay between experimental results and numerical simulations has improved the understanding of the displacement process. It has been shown that the different structures observed when changing the physical parameters of the fluids like viscosity contrast, wettability, interfacial tension and displacement rate [1–6] divide into three flow regimes. These three major regimes are referred to as viscous fingering [1,2] stable displacement [3] and capillary fingering [7]. There exist statistical models such as DLA [8], anti-DLA [9] and invasion percolation [10] that reproduce the basic domains in viscous fingering, stable displacement and capillary fingering respectively. However, these models do not contain any physical time for the front evolution and they cannot describe the crossover between the different flow regimes.

Much effort has gone into making better models whose properties are closer to that of real porous media. This has resulted in several network simulators, modeling fluid flow on a lattice of pores and throats [2,3,11–19]. Most of the network models have been used to obtain new information on the different flow regimes and to study the statistical properties of the displacement structures. Some others, have been used to calculate macroscopic properties like fluid saturations and relative permeabilities and compare them with corresponding experimental data. However, to our knowledge no network model has been capable of simulating the dynamics of the fluid pressures during the displacement process. This is the goal of the present work.

We have simulated the temporal evolution of the pressure in all the three regimes of interest: viscous fingering, stable displacement and capillary fingering. The injection rate in the displacements has been systematically varied and we have analyzed the behavior of the pressure in the crossover between the three regimes. Moreover, we discuss what effect trapped clusters have on the evolution of the pressure in the system and we relate the data to macroscopic

*Also at: Norwegian University of Science and Technology, N-7034 Trondheim, Norway

†Also at: IKU Petroleum Research, N-7034 Trondheim, Norway

flow equations. We find that capillary forces play an important role in two-phase flow at both high and low injection rates.

The paper is organized as follows. In Sec. II we present the network model, in Sec. III we show the simulation results and in Sec. IV we present our conclusions and related the findings to macroscopic quantities.

II. THE NETWORK MODEL

The network model has been presented in [20] and we will restrict ourself to a short sketch here.

A. Geometry and boundary conditions

The porous medium is represented by a square lattice tubes connected at the nodes. At each node four tubes meet and there is no volume assigned to the nodes: the tubes represent the volume of both pores and throats. The tubes are cylindrical with length d . Each tube is assigned an average radius r which is chosen at random in the interval $[\lambda_1 d, \lambda_2 d]$, where $0 \leq \lambda_1 < \lambda_2 \leq 1$. The randomness of the radii represents the disorder in the model.

The liquids flow from the bottom to the top of the lattice and we implement periodic boundary conditions in the horizontal direction. The pressure difference between the bottom row and the top row defines the pressure across the lattice. Gravity effects are neglected, and consequently we consider horizontal flow in a two-dimensional network of tubes.

B. Fluid flow through the network

Initially, the system is filled with a defending fluid with viscosity μ_1 . The invading fluid with viscosity μ_2 is injected along the bottom row with a constant injection rate. We model drainage, i.e. the invading fluid is non-wetting and the defending fluid is wetting. Furthermore, we assume that the fluids are incompressible and immiscible. Consequently, the volume flux is conserved everywhere in the lattice and a well defined interface develops between the two phases.

The capillary pressure p_c due to the interface between the non-wetting and wetting fluid inside a tube (a meniscus) is given by the Young-Laplace law

$$p_c = \frac{2\gamma}{r} \cos \theta . \quad (1)$$

Here r is the radius of the tube, γ is the interfacial tension and θ denotes the wetting angle between the non-wetting and wetting phases. θ is in the interval $(0, \pi/2)$ for drainage displacements.

We assume that the tubes are hour glass shaped where the effective radii of the tubes follow a smooth function. Thus, the capillary pressure becomes a function of the position of the meniscus in the tube and we assume that the Young-Laplace law (1) takes the form

$$p_c = \frac{2\gamma}{r} [1 - \cos(2\pi\hat{x})] . \quad (2)$$

Here \hat{x} is the dimensionless value of the meniscus' position in the tube ($0 \leq \hat{x} \leq 1$), and $\theta = 0$ (perfect wetting). From Eq. (2) $p_c = 0$ at the ends of the tube while p_c approaches its maximum of $4\gamma/r$ in the middle of the tube.

The volume flux q_{ij} through a tube from the i th to the j th node in the lattice (Fig. 1) is found from the Washburn equation for capillary flow [21]. As an approximation we treat the tubes as if they were cylindrical and obtain

$$q_{ij} = -\frac{\pi r_{ij}^2 k_{ij}}{\mu_{eff}} \cdot \frac{1}{d} (\Delta p_{ij} - \tilde{p}_c) . \quad (3)$$

Here k_{ij} is the permeability of the tube given by $k_{ij} = r_{ij}^2/8$ where r_{ij} is the average radius of the tube. $\Delta p_{ij} = p_j - p_i$ is the pressure difference between the i th and j th node. A tube partially filled with both of the liquids is allowed to contain either one or two menisci leading to four different arrangements as shown in Fig. 2. The effective viscosity of those tubes, denoted as μ_{eff} in Eq. (3), becomes a sum of the amount of each fluid multiplied by their respective viscosities. The total capillary pressure, \tilde{p}_c in Eq. (3), is the sum of the capillary pressures of the menisci that are inside the tube. The absolute value of the capillary pressure of each meniscus is given by Eq. (2), while its sign depends on whether the meniscus is pointing upwards like in Fig. 2 (a) or downwards like in Fig. 2 (b). In the simple case where the tube only contains one meniscus (Fig. 1) $\mu_{eff} = \mu_2 \hat{x}_{ij} + \mu_1 (1 - \hat{x}_{ij})$ and $\tilde{p}_c = p_c$. For a tube without menisci $\tilde{p}_c = 0$, and Eq. (3) reduces to that describing Hagen-Poiseuille flow with $\mu_{eff} = \mu_1$ or μ_2 .

C. Determining the flow field

There is no volume assigned to the nodes giving conservation of volume flux at each node

$$\sum_j q_{ij} = 0 . \quad (4)$$

The summation on j runs over the nearest neighbor nodes to the i th node while i runs over all nodes that do not belong to the top or bottom rows, that is, the internal nodes.

Eqs. (3) and (4) constitute a set of linear equations which are to be solved for the nodal pressures p_j with the constraint that the pressures at the nodes belonging to the upper and lower rows are kept fixed. The set of equations is solved by using the Conjugate Gradient method [22].

We want to study the dynamics of the pressure fluctuations at constant displacement rate. Therefore, we need to find the pressure across the lattice for a desired injection rate and then use that pressure to solve fluid flow through the network. For two-phase displacement the pressure across the lattice ΔP is related to the injection rate Q through the equation

$$Q = A\Delta P + B . \quad (5)$$

Here A and B are parameters depending on the geometry of the medium and the current configuration of the liquids. The first part of Eq. (5) is simply Darcy's law for one phase flow, while the last part B results from the capillary pressure between the two phases. As long as the menisci do not move B is constant.

The pressure Δp_{ij} across each tube can be related to the pressure across the lattice ΔP . All the equations calculating the fluid flow in the system, have the functional form $f(x) = ax + b$. As a consequence Δp_{ij} becomes a function of ΔP ,

$$\Delta p_{ij} = \Gamma_{ij}\Delta P + \Pi_{ij} . \quad (6)$$

Γ_{ij} is a dimensionless quantity depending on the mobilities (k/μ_{eff}) of the tubes and Π_{ij} is a function of the capillary pressures of the menisci inside the tubes. If no menisci are present Π_{ij} is zero. Eq. (6) can easily be deduced for two cylindrical tubes with different radii connected in series.

By inserting Eq. (6) into Eq. (3) we obtain after some algebra a relation between the local flow rate q_{ij} and the pressure ΔP across the network

$$q_{ij} = \tilde{a}_{ij}\Delta P + \tilde{b}_{ij} . \quad (7)$$

The parameter \tilde{a}_{ij} is proportional to Γ_{ij} and the mobility (k_{ij}/μ_{eff}) of the tube ij . \tilde{b}_{ij} contains the capillary pressures of the menisci.

The solution due to a constant injection rate can now be summarized into the following steps:

1. We first find the nodal pressures for two different pressures $\Delta P'$ and $\Delta P''$ applied across the lattice.
2. From the two solutions of the nodal pressures the corresponding injection rates Q' and Q'' and the local flow rate q'_{ij} and q''_{ij} are calculated.
3. A and B is calculated by solving the two equations obtained when inserting $\Delta P'$, Q' , $\Delta P''$ and Q'' into Eq. (5).
4. The pressure ΔP across the lattice for the desired Q is then calculated by using Eq. (5).
5. This ΔP is inserted in Eq. (7) to get the local flow q_{ij} . Note that the parameters \tilde{a}_{ij} and \tilde{b}_{ij} must first be found by solving the two equations obtained by inserting q'_{ij} , $\Delta P'$, q''_{ij} and $\Delta P''$ from step 2 into Eq. (7).

D. Moving the menisci

A time step Δt is chosen such that every meniscus is allowed to travel at most a maximum step length Δx_{max} during that time step. In each time step we check whether or not a meniscus crosses a node. If this happens, the time step is redefined such that this meniscus stops at the end of the tube.

A meniscus reaching the end of a tube is moved into the neighbor tubes according to some defined rules. These rules take care of the different fluid arrangements that can appear around the node. Basically, the non-wetting fluid can either invade into or retreat from the neighbor tubes as shown in Fig. 3(a) and (b) respectively. In Fig. 3(a) the non-wetting fluid approaches the node from below (drainage). When the meniscus has reached the end of the tube (position 1), it is removed and three new menisci are created at position δ in the neighbor tubes (position 2). The

distance δ is about 1–5% of the tube length d . The small distance δ avoids that the created menisci at position 2 immediately disappear and move back to the initial position 1 in tubes where the flow direction is opposite to the direction of the invading fluid. The total time lapse is adjusted to compensate the instantaneous change in local volume of the fluids when the menisci move a distance δ . The time lapse is adjusted such that the total volume of the fluids always is conserved.

Fig. 3 (b) shows the opposite case when the non-wetting fluid retreats into a single tube (imbibition). As Fig. 3 (b) shows the properties of imbibition should not be neglected as long as the menisci can travel in both directions. Our approximation in Fig. 3 (b) cannot handle important properties found in imbibition such as film flow and snap off [5,23]. However, in drainage which is what we are focusing on, arrangement (b) will appear rarely compared to (a). For that reason, any further description of imbibition than the one presented in Fig. 3 (b), does not seem necessary.

Summarized, the procedure for each time step Δt is:

1. The nodal pressures p_j are determined.
2. The p_j 's are related to the desired injection rate Q from Eqs. (5) and (7).
3. The local flow rate in each tube is computed by using Eq. (3).
4. The local flow rates are used to calculate the time step Δt such that only one meniscus reaches the end of a tube or travel at most the step length Δx_{max} during that time step.
5. The menisci are updated according to Δt . The total time lapse is recorded before the whole procedure is repeated for the new fluid configuration.

III. SIMULATIONS

In two-phase fluid displacement there are mainly three types of forces: viscous forces in the invading fluid, viscous forces in the defending fluid and capillary forces due to the interface between them. This leads to two dimensionless numbers that characterize the flow: the capillary number C_a and the viscosity ratio M .

The capillary number describes the competition between capillary and viscous forces. It is defined as

$$C_a = \frac{Q\mu}{\Sigma\gamma}, \quad (8)$$

where Q (cm²/s) denotes the injection rate, μ (Poise) is the maximum viscosity of the two fluids, Σ (cm²) is the cross section of the inlet and γ (dyn/cm) is the interfacial tension between the two phases. Σ is calculated by taking the product of the length of the inlet and the mean thickness of the lattice due to the average radius of the tubes.

M defines the ratio of the viscosities of the two fluids and is given by the invading viscosity μ_2 divided with the defending viscosity μ_1 :

$$M = \frac{\mu_2}{\mu_1}. \quad (9)$$

In the simulations the pressure across the lattice ΔP is given by Eq. (5) as

$$\Delta P = \frac{Q}{A} - \frac{B}{A} = \frac{Q}{A} + P_{cg}. \quad (10)$$

Since B is due to the capillary pressure of the menisci, we define $-B/A$ as the global capillary pressure of the system, P_{cg} . P_{cg} includes the menisci surrounding the trapped cluster of defending fluid (cluster menisci) as well as the menisci belonging to the front between the invading and defending fluid (front menisci).

In addition to P_{cg} we calculate P_{cf} , the capillary pressure averaged along the front. P_{cf} consists only of the capillary pressures due to the front menisci and we define it as

$$P_{cf} = \frac{1}{N} \sum_{\alpha=1}^N |p_c^\alpha|. \quad (11)$$

Here the index α addresses the tubes in the lattice and in the summation α runs over all tubes containing a meniscus that belong to the front. N is the number of such tubes. p_c^α is the capillary pressure of the front meniscus in tube α . See Fig. 4 for an example of a structure obtained after a simulation with low capillary number. The tubes containing a front meniscus or belonging to the trapped cluster of defending fluid are identified by running a Hoshen-Kopelman algorithm [24] on the lattice.

The displacement structure in Fig. 4 shows that the front is a complicated path connecting the left and the right boundaries of the lattice. The width of the front w is found by taking the standard deviation of the distances between all the front tubes and the average position of the front.

For every simulation we have calculated ΔP and P_{cg} as functions of time. For some of the simulations we have also computed the average capillary pressure P_{cf} along the front and analyzed the behavior of A in Eq. (5). As will be discussed below, ΔP , P_{cg} and P_{cf} are strongly correlated and A seems to obey surprisingly simple relations.

We have performed drainage simulations in each of the regimes of interest: viscous fingering, stable displacement and capillary fingering with $M = 1.0 \times 10^{-3}$, 1.0 and 1.0×10^2 respectively. The injection rate was systematically varied for each of the viscosity ratios. The simulations were performed with parameters as close as possible to experiments performed in [25]. The length d of all tubes in the lattices were set equal to 1 mm and the radii r of the tubes were chosen randomly in the interval $0.05d \leq r \leq d$. The interfacial tension was set to $\gamma = 30$ dyn/cm and the viscosities of the defending and the invading fluids varied between 0.01 P (\simeq water) and 10 P (\simeq glycerol).

A. Viscous fingering, $M < 1$

Our study of this regime consists of a series of simulations with constant viscosity ratio $M = 1.0 \times 10^{-3}$. The injection rates and the capillary number used in the different simulations are listed in Table I. To save computation time, most of the simulations were performed on a lattice of 25×35 nodes. However, one was performed on a lattice of 60×80 nodes and the resulting structure of this simulation is shown in Fig. 5.

In viscous fingering the principal force is due to the viscous forces in the defending fluid. The pattern formation in Fig. 5 shows that the invading fluid creates typical fingers into the defending fluid. The pressure across the lattice, ΔP , shown in Fig. 6, decreases as the less viscous fluid invades the system. The slope of the average decreasing pressure function is non-trivial and results from the fractal development of the fingers.

The global capillary pressure P_{cg} , also shown in Fig. 6, fluctuates around a mean value of about 1×10^3 dyn/cm². The fluctuation is strongly correlated in both time and amplitude to the noise in ΔP . As will be discussed below, the variations correspond to the changes in the capillary pressure as a meniscus invades into or retreats from a tube.

We have calculated P_{cf} for every simulation performed on the lattices of 25×35 nodes. The result for four of the simulations is shown in Fig. 7 together with the global capillary pressure P_{cg} . The pressures in Fig. 7 are normalized by dividing them with the average threshold pressure of the tubes. The average threshold pressure is defined as $2\gamma/\langle r \rangle$ where $\langle r \rangle$ is the mean radius of the tubes. The mean threshold pressure is about 1.1×10^3 dyn/cm² in all simulations, since the radii of the tubes always are chosen randomly in the interval [0.05, 1.0] mm. Note that in Fig. 7, P_{cg} has been subtracted by 1000 dyn/cm² before it was normalized. This avoids the pressure functions to overlap at low capillary numbers when they are plotted in the figure.

Fig. 7 shows that the fluctuations of P_{cf} are correlated in time to the fluctuations of P_{cg} . At lowest $C_a = 3.5 \times 10^{-4}$, P_{cf} and P_{cg} are even indistinguishable. For all simulations except that at lowest capillary number the amplitude of the fluctuations in P_{cf} decreases as time increases. For high injection rates P_{cf} is found to approach 1, which is the mean threshold pressure.

In the simulation at $C_a = 3.5 \times 10^{-4}$ we approach the regime of capillary fingering. In slow capillary fingering the local capillary pressures of the menisci becomes equal when all the menisci are stable. This is often referred to as capillary equilibrium leading to $P_{cg} \simeq P_{cf}$. However, in fast displacement the local capillary pressures are generally different. Thus, for a large system with many menisci the average capillary pressure of the front will approach the average threshold pressure of the tubes.

Due to the less viscous defending fluid the pressure gradient at high injection rate is largest at the finger tip closest to the upper boundary of the lattice. The meniscus in the uppermost finger tip will therefore more likely continue and invade the next tube compared to the menisci lying behind it. Thus, the menisci lying behind will get stuck and the fluctuations in the global capillary pressure can only be caused by the moving finger tip. This is seen in Fig. 8 where we have plotted P_{cg} (a) together with the capillary pressure of the meniscus which is located in the tube that always has the largest flow rate. The data in Fig. 8 are taken from the simulation performed at $C_a = 1.1 \times 10^{-2}$ given in Table I.

On basis of Figs. 7 and 8 we conclude that the fluctuations in P_{cg} correspond to the local capillary pressure of the menisci invading the tubes. Moreover, the average level of P_{cg} is almost equal P_{cf} .

B. Stable displacement, $M > 1$

In the regime of stable displacement we have run seven simulations spread over different lattices of size between 25×35 and 60×60 nodes. See Table II. The simulations were run with the viscosity ratio $M = 1.0 \times 10^2$, but at different capillary numbers. The resulting structure of a simulation performed on a lattice with 60×60 nodes is visualized in Fig. 9. The pressure across the lattice ΔP , the global capillary pressure P_{cg} and $1/A$ were calculated for all simulations. The results are plotted in Figs. 10 and 11 .

In stable displacements the fluid movements are dominated by the viscous forces in the invading liquid. The viscous pressure gradient in the invading phase is found to stabilize the front and a compact pattern with an almost flat front between the non-wetting and wetting fluid is generated (see Fig. 9). The stabilized front introduces a length scale in the system for large times. This length scale is identified as the saturation width w_s of the front [25].

To save computation time the simulations performed on the lattices of 40×40 and 60×60 nodes (Fig. 10) were stopped after the width of the front had stabilized. The other simulations (Fig. 11), however, were run until the invading fluid reached the outlet.

The pressures in Figs. 10 and 11 show a quite different behavior compared to the pressures in Figs. 6 and 7. The pressure across the lattice ΔP (a) and the global capillary pressure P_{cg} (b) are both found to increase as the more viscous fluid is injected into the system. However, the average slope depend very much on the injection rate. At low capillary numbers ($C_a = 7.5 \times 10^{-4}$) we reach the regime of capillary fingering and similar to viscous fingering the pressures reduce to that describing the capillary fluctuations along the front.

To explain the rather unexpected behavior at high injection rates we have to discuss the effect of the trapped cluster of the defending fluid left behind the front. In stable displacement the driving pressure gradient lies between the inlet and the front causing a pressure drop between the top and the bottom of the trapped clusters. At moderate injection rates where the clusters stay in place and keep their shapes, the forces due to the pressure drop must be canceled by capillary forces acting on the cluster menisci. The sum of those capillary forces contribute to the observed increase in P_{cg} .

The above interpretation of P_{cg} also applies in the regime of viscous fingering. In viscous fingering at high capillary numbers there are few clusters. Thus, the extra contribution to P_{cg} from the cluster menisci becomes negligible. When the injection rate is reduced clusters develop, but now the pressure gradient across the clusters is small because of the low injection rate. Therefore, the contribution to P_{cg} still is negligible. This is in agreement of the observations in the previous section where P_{cg} was found to fluctuate around a constant level for both high and low capillary numbers.

All the displacements listed in Table II, except that at $C_a = 7.5 \times 10^{-4}$, reached the saturation time t_s where the front stabilize. In Figs. 10 and 11 t_s is indicated by a vertical dashed line. If we neglect the fluctuations, ΔP and P_{cg} are approximately linear functions of time for $t > t_s$.

The linearity in P_{cg} is explained by looking at the generation of the clusters in the system. We notice that for large times ($t > t_s$), when the front has saturated with fully developed clusters behind it, the average front position h can only depend on the injection rate and the viscosity ratio. Both properties are constant through each simulation, resulting in h being linear in time. A plot showing the average front position as a function of time at $C_a = 4.6 \times 10^{-3}$ for the lattice with 60×60 nodes is shown in Fig. 12.

On average, every cluster contributes to P_{cg} with a certain amount causing the global capillary pressure to be proportional to the number of clusters behind the front. For large times, the number of clusters increases linearly with the average front position causing P_{cg} to be linear in h . Summarized we obtain

$$P_{cg} \propto h \propto t \quad , \quad t > t_s . \quad (12)$$

It has to be emphasized that there might be large deviations from the observed linearities when clusters of size comparable to the system develops. The argument does not apply when $t < t_s$, either. Then the average change in ΔP and P_{cg} depends on the fractal development of the displacement structure.

The quantity $1/A$, defined in Eq. (5), is calculated by using Eq. (10). In Figs. 10 and 11 we have plotted A_0/A expressed as

$$\frac{A_0}{A} = A_0 \frac{\Delta P - P_{cg}}{Q} . \quad (13)$$

Here A_0 is equal to the proportionality factor between Q and ΔP when only the defending fluid flows trough the lattice, i.e. $A_0 = \Sigma K / \mu_1 L$. K denotes the absolute permeability of the lattice and L is the length of the system. From Figs. 10 and 11, we conclude that at high capillary numbers and for $t > t_s$, $1/A$ is proportional to the injection time.

The linearity in $1/A$ is related to the displacement structure that develop during injection of non-wetting fluid. Let us return to equation Eq. (5) which we can rewrite to obtain

$$Q = \Sigma G (\Delta P - P_{cg}) \frac{1}{L}, \quad (14)$$

where $G \equiv AL/\Sigma$ defines the simulated mobility of the system. It must be emphasized that this mobility may be hard to measure experimentally and it should not be confused with the conventional effective mobility of the system, denoted by G_{eff} (see below). Eq. (14) looks very similar to Eq. (3) describing the fluid flow through a single tube. If we now assume that an equation of the form (3) applies on the whole lattice we interpret G as

$$G = \frac{K}{\mu_{eff}}. \quad (15)$$

Here μ_{eff} is the effective viscosity of the whole system. μ_{eff} is not trivial to calculate because of the fractal structure of the trapped clusters and front. However, if we denote the normalized average front position as \hat{h} and assume that the viscosity of the region behind the front can be expressed by an effective viscosity μ_2' , μ_{eff} becomes

$$\mu_{eff} = (1 - \hat{h})\mu_1 + \hat{h}\mu_2'. \quad (16)$$

Here $0 < \hat{h} < 1$. By combining Eqs. (16) and (15), we finally obtain after some reorganization

$$\frac{1}{G} \propto \frac{1}{A} = \frac{1}{A_0} \left[(M_e - 1)\hat{h} + 1 \right], \quad (17)$$

where $M_e \equiv \mu_2'/\mu_1$ defines the effective viscosity ratio.

To a first approximation, we have calculated μ_2' directly from the displacement structure by taking the sum of the fluid viscosities multiplied by their respective macroscopic saturations behind the front. However, the calculated μ_2' was not consistent with $(M_e - 1)$ given by the average slope of A_0/A plotted in Figs. 10 and 11. This indicates that μ_2' not only depend on the fluid saturations but also the structure of the liquids behind the front. Thus, microscopic properties of the fluid configurations has to be considered in order to find the correct M_e .

We are now in a position to derive a more exact formalism describing the pressure evolution and the changes in the effective mobility G_{eff} of the system when clusters develop. G_{eff} corresponds to the ratio of the effective permeability and the effective viscosity of the system. If we again look at the global capillary pressure P_{cg} , it can be interpreted as a sum of the capillary pressure along the front menisci, P_{mf} and the capillary pressure of the cluster menisci, P_{mc} . Furthermore, for large times ($t > t_s$) we can express $P_{mc} = \Delta_{mc} h$ giving

$$P_{cg} = \Delta_{mc} h + P_{mf}. \quad (18)$$

Here Δ_{mc} denotes the proportionality factor between P_{cg} and h where $0 < h < L$ is the average front position. In the limit of very low injection rate the capillary pressure of the front and cluster menisci will approach capillary equilibrium causing $\Delta_{mc} \rightarrow 0$ and $P_{mf} \simeq P_{cf} \simeq P_{cg}$.

We can use the relation for P_{cg} in Eq. (18) to deduce a formula for G_{eff} . What we are seeking is an equation for the flow rate U , on the form of Darcy's law

$$U = G_{eff} (\Delta P - P_{mf}) \frac{1}{L}. \quad (19)$$

The pressure gradient $(\Delta P - P_{mf})/L$ accounts for the capillary pressure due to the front, P_{mf} .

We start by inserting Eq. (18) into Eq. (14) to get

$$U = \frac{K}{\mu_{eff}} (\Delta P - \Delta_{mc} h - P_{mf}) \frac{1}{L}, \quad (20)$$

where the flow velocity $U \equiv Q/\Sigma$. Eq. (20) can be written into the form of Darcy's to obtain

$$U = \frac{K}{\mu_{eff} + \mu_{mc}} (\Delta P - P_{mf}) \frac{1}{L}, \quad (21)$$

where

$$\mu_{mc} \equiv \frac{K}{UL} \Delta_{mc} h. \quad (22)$$

From Eq. (21) we immediately interpret μ_{mc} as the increase in viscosity of the invaded region caused by the cluster formation. However, this may just as well be seen as a decrease in the effective permeability behind the front [25]. Note that the U dependency in Eq. (22) only indicates changes in Δ_{mc} between displacements executed at different injection rates. The behavior when the flow rate changes during one displacement is not discussed here. From Eq. (21) we finally define the effective mobility of the lattice as

$$G_{eff} \equiv \frac{K}{\mu_{eff} + \mu_{mc}}. \quad (23)$$

There is one important interpretation of G_{eff} when the average front position has reached the outlet, i.e. $h = L$. Then only the invading fluid flows through the system and G_{eff} becomes equal to the effective mobility of the invading phase. If we insert Eqs. (16) and (22) into Eq. (23) we obtain when $h = L$

$$G_{eff}(h = L) = \frac{K}{\mu_2' + \frac{K\Delta_{mc}}{U}}. \quad (24)$$

From this expression follows directly a relation for the relative permeability of the invading phase, k_{ri} defined as

$$k_{ri} = \frac{G_{eff}(h = L)\mu_2'}{K}. \quad (25)$$

Note that $\mu_2' = \mu_{eff}(\hat{h} = 1)$ from Eq. (16) and that μ_2' is given by the slope of $1/A$ in Eq. (17).

The above formalism resulting in Eq. (23), takes into account the capillary pressure of the cluster menisci as well as the capillary pressure along the front. However, at moderate injection rates where the clusters stay in place and keep their shapes, we have found G_{eff} directly in the simulations by assigning zero permeability to tubes belonging to the trapped clusters. Thus, the clusters will be frozen to their initial positions and in the calculations they are treated as additional boundary conditions where fluid cannot flow. Simulations have provided evidence that when the clusters are frozen the parameter A in Eq. (5) adjusts such that the simulated G in Eq. (14) becomes equal to the calculated G_{eff} in Eq. (23). G_{eff} is calculated by using P_{cg} and ΔP which are plotted in Figs. 10 and 11. Moreover, with frozen clusters the global capillary pressure P_{cg} , reduces to that describing the capillary pressure along the front, P_{mf} .

C. Capillary fingering, $M = 1$

In the regime of capillary fingering we have run 17 simulations with viscosity matching fluids ($M = 1.0$) spread over six different capillary numbers. The different capillary numbers and the corresponding injection rates are listed in Table III. The lattice size was 40×60 nodes for all simulations. Due to long computation time we only did two simulations at the lowest capillary number. For all the other capillary numbers, we ran three simulations.

In capillary fingering the displacement is so slow that the viscous forces are negligible, with the consequence that the main force is the capillary one between the two fluids. Only the strength of the threshold pressure in a given tube decides whether the invading fluid invades that tube or not. Since the radii of the tubes (which determine the threshold pressures) are randomly chosen from a given interval, the non-wetting fluid flows along the path of least resistance.

The displacement structure of one of the simulations at lowest $C_a = 4.6 \times 10^{-5}$ is shown in Fig. 4. We observe that the invading fluid creates a rough front with trapped clusters that appear at all scales between the tube length and the maximum width of the front.

For all simulations ΔP and P_{cg} were calculated. The result for six of the simulations each at one of the different capillary numbers are shown in Fig. 13. In the figure (a) denotes ΔP and (b) denotes P_{cg} . Note that P_{cg} has been subtracted by 1000 dyn/cm^2 to avoid overlap of the curves at low capillary numbers.

The front was found to stabilize at high injection rates [25] and the saturation time t_s is indicated by the vertical dashed line in Fig. 13. At the lowest capillary number it might be difficult to estimate the saturation time accurately. At very low injection rate the width of the front probably approaches an upper cut off equal to the finite size of the lattice.

At high capillary numbers for $t > t_s$, ΔP and P_{cg} are found to increase linearly as a function of time. This is consistent with the result from stable displacement. However, the difference $\Delta P - P_{cg}$, is constant through each of the simulation opposed to what we observed when $M > 1$. Fig. 14 shows the difference $\Delta P - P_{cg}$ for one of the simulations at $C_a = 2.3 \times 10^{-4}$. The plot shows the normalized value of $\Delta P - P_{cg}$ subtracted by 1 such that the resulting data fall close to zero. The fluctuations appearing in the 9th digit are caused by numerical round off errors in the simulations.

In the previous section we suggested that the mobility G defined in Eq. (15), was a function of the effective viscosity μ_{eff} . Moreover, we assumed that μ_{eff} depends on the saturation of the invading and the defending fluid and the displacement structure. When $\mu_1 = \mu_2$ none of these assumptions apply. From Eq. (14) the constant pressure difference $\Delta P - P_{cg}$ in Fig. 14 implies that the simulated mobility G becomes constant, even with respect to the local displacement structure. The effective viscosity reduces to the viscosity of the two liquids, $\mu_{eff} = \mu_1 = \mu_2$ giving $A = A_0 = \Sigma K / \mu_1 L$. The difference $\Delta P - P_{cg}$, however, depend on the injection rate Q . This is observed in Fig. 13 where $\Delta P - P_{cg}$ increases for increasing capillary number.

When $\mu_1 = \mu_2$ the pressure difference $\Delta P - P_{cg}$ has a simple interpretation. It corresponds to the viscous pressure drop arising when viscous fluids are moving. When the injection rate is reduced the viscous pressure drop becomes negligible and we approach the regime of capillary fingering. At low injection rates the pressure gradient across the trapped clusters also vanish giving only a small increase in ΔP and P_{cg} . This is observed in Fig. 13 at $C_a = 4.6 \times 10^{-5}$ where the average increase in P_{cg} becomes quite small and $\Delta P \simeq P_{cg}$. In the same figure, the sudden jumps in the pressure function identify the bursts where the invading fluid proceeds abruptly. This corresponds to Haines jumps [26,27].

The property that the mobility G is constant when the liquids have equal viscosities simplifies the computation of the nodal pressures in the lattice. By substituting A with A_0 in Eq. (5) we find that the injection rate is given by

$$Q = A_0 \Delta P + B . \quad (26)$$

This equation has only one unknown, the term B , opposed to the original Eq. (5) having two unknowns, both A and B . To verify the result when A is replaced by A_0 we have compared the solution found from Eq. (26), necessitating one solution of the flow equations, with the one given when Eq. (5) is solved twice. Not surprisingly, there is excellent agreement between these two results.

The strong evidence that $A = A_0$ is constant in Eq. (26) can be deduced from simple considerations of the energy dissipation in the system. In analogy with electrical circuits, we define the total energy dissipation W in the system as

$$W = Q \Delta P . \quad (27)$$

The total dissipation must equals the sum of the dissipation in every tube α in the lattice. Thus,

$$Q \Delta P = \sum_{\alpha} q_{\alpha} \Delta p_{\alpha} , \quad (28)$$

where the summation index α runs over all tubes in the lattice. q_{α} is given by Eq. (3) which we rewrite as ($ij \rightarrow \alpha$)

$$q_{\alpha} = a_{\alpha} \Delta p_{\alpha} + b_{\alpha} . \quad (29)$$

Here we note that a_{α} is proportional to k_{α} / μ_{eff} , the mobility of the tube α . By inserting Eq. (5) and (29) into Eq. (28) we get after some reorganization

$$A \Delta P + B = \sum_{\alpha} a_{\alpha} \Delta P \left(\frac{\Delta p_{\alpha}}{\Delta P} \right)^2 + b_{\alpha} \frac{\Delta p_{\alpha}}{\Delta P} . \quad (30)$$

By replacing the local pressure Δp_{α} in Eq. (30) with ΔP , using Eq. (6) we obtain after some algebra

$$Q = \left[\sum_{\alpha} a_{\alpha} \Gamma_{\alpha}^2 \right] \Delta P + \left[\sum_{\alpha} \Gamma_{\alpha} (2a_{\alpha} \Pi_{\alpha} + b_{\alpha}) + \frac{\Pi_{\alpha}}{\Delta P} (a_{\alpha} \Pi_{\alpha} + b_{\alpha}) \right] . \quad (31)$$

If we compare the above equation with Eq. (5) we recognize the first summation as A and the second as B . Thus, A depends entirely on a_{α} and Γ_{α} . As stated earlier, both a_{α} and Γ_{α} are proportional to the mobility of the tubes. The mobility of each tube depends on the local fluid configurations, through the effective viscosity μ_{eff} as defined in Eq. (16). However, when the fluids have equal viscosities we get $\mu_{eff} = \mu_1 = \mu_2$. As a consequence a_{α} and Γ_{α} becomes constant, which is consistent with the simulation result.

IV. DISCUSSIONS

We have simulated drainage displacements at different injection rates for three different viscosity ratios $M = 1.0 \times 10^{-3}$, 1.0 and 1.0×10^2 . The main focus of the work is the study of the temporal evolution of the pressure when a non-wetting fluid displaces a wetting fluid in porous media. Moreover, the effect of the trapped clusters on the displacement process has been discussed. From the results we clearly see that the capillary forces play an important role at both high and low injection rates.

At high injection rates with $M \geq 1.0$ the global capillary pressure, P_{cg} was found to increase as a function of the number of trapped clusters behind the front. For large times when the front has saturated, P_{cg} becomes even proportion to the average front position h . This lead to a formalism describing the evolution of the effective mobility when the non-wetting fluid was injected into the system. Moreover, we showed that this effective mobility could be used to estimate the relative permeability of the invading phase when the average front position has reached the outlet.

At moderate injection rates the effective mobility given by P_{cg} , were shown to be equivalent to assigning zero permeability to tubes belonging to the trapped clusters. When $M \ll 1.0$ or at low injection rates the effect of the clusters become negligible reducing P_{cg} to describe the local capillary fluctuations of the invading menisci along the front. With displacements performed with equal viscosities, $M = 1.0$, we found that the difference $\Delta P - P_{cg}$ was constant. This was shown to be consistent with the energy dissipation in the system.

It must be emphasized that the properties we report are only valid for drainage. So far the model is not capable to simulate imbibition. The simulations have also been performed on a two-dimensional porous system where clusters develop more easily, compared to fluid flow in three-dimensional porous media [28]. Moreover, the lattice sizes are limited by the computation time and more sophisticated and efficient algorithms have to be developed in order to increase the system sizes and thereby improve the above results. Another, and not less important exercise is to compare our simulation results with experimental measurements.

ACKNOWLEDGMENTS

The authors thank S. Basak, G. G. Batrouni, E. G. Flekkøy and J. Schmittbuhl for valuable comments. The work is supported by NFR, the Norwegian Research Council, through a “SUP” program and a grant of computation time. The work has also got computer time from the Idris in Paris and from HLRZ, Forschungszentrum Jülich GmbH.

-
- [1] K. J. Måløy, J. Feder, and T. Jøssang, *Phys. Rev. Lett.* **55**, 26881 (1985).
 - [2] J.-D. Chen and D. Wilkinson, *Phys. Rev. Lett.* **55**, 1892 (1985).
 - [3] R. Lenormand, E. Touboul, and C. Zarcone, *J. Fluid Mech.* **189**, 165 (1988).
 - [4] M. Cieplak and M. O. Robbins, *Phys. Rev. Lett.* **60**, 2042 (1988).
 - [5] M. Cieplak and M. O. Robbins, *Phys. Rev. B.* **41**, 11508 (1990).
 - [6] N. Martys, M. Cieplak, and M. O. Robbins, *Phys. Rev. Lett.* **66**, 1058 (1991).
 - [7] R. Lenormand and C. Zarcone, *Phys. Rev. Lett.* **54**, 2226 (1985).
 - [8] T. A. Witten and L. M. Sander, *Phys. Rev. Lett.* **47**, 1400 (1981).
 - [9] L. Paterson, *Phys. Rev. Lett.* **52**, 1621 (1984).
 - [10] D. Wilkinson and J. F. Willemsen, *J. Phys. A* **16**, 3365 (1983).
 - [11] J. Koplik and T. J. Lasseter, *SPEJ* **22**, 89 (1985).
 - [12] M. M. Dias and A. C. Payatakes, *J. Fluid Mech.* **164**, 305 (1986).
 - [13] P. R. King, *J. Phys. A* **20**, L529 (1987).
 - [14] M. Blunt and P. King, *Phys. Rev. A* **42**, 4780 (1990).
 - [15] M. Blunt and P. King, *Transp. Porous Media* **6**, 407 (1991).
 - [16] P. C. Reeves and M. A. Celia, *Water Resour. Res.* **32**, 2345 (1996).
 - [17] G. N. Constantinides and A. C. Payatakes, *AIChE Journal* **42**, 369 (1996).
 - [18] E. W. Pereira, W. V. Pinczewski, D. Y. C. Chan, L. Paterson, and P. E. Øren, *Transp. Porous Media* **24**, 167 (1996).
 - [19] D. H. Fenwick and M. J. Blunt. *SPE 38881, proc. of the SPE Annual Tech. Conf.*, San Antonio, Texas, U.S.A., Oct. 1997.
 - [20] E. Aker, K. J. Måløy, A. Hansen, and G. G. Batrouni, “A two-dimensional network simulator for two-phase flow in porous media”. Submitted to *Transp. Porous Media*, 1997.

- [21] E. W. Washburn, *Phys. Rev.* **17**, 273 (1921).
- [22] G. G. Batrouni and A. Hansen, *J. Stat. Phys.* **52**, 747 (1988).
- [23] R. Lenormand, C. Zarcone, and A. Sarr, *J. Fluid. Mech.* **135**, 337 (1983).
- [24] D. Stauffer and A. Aharony. *Introduction to percolation theory*. Taylor & Francis, London, Great Britain, 1992.
- [25] O. I. Frette, K. J. Måløy, J. Schmittbuhl, and A. Hansen, *Phys. Rev. E.* **55**, 2969 (1997).
- [26] W. B. Haines, *J. Agr. Sci.* **20**, 97 (1930).
- [27] K. J. Måløy, L. Furuberg, J. Feder, and T. Jøssang, *Phys. Rev. Lett.* **68**, 2161 (1992).
- [28] D. Wilkinson, *Phys. Rev. A* **34**, 1380 (1986).

FIG. 1. Flow in a tube containing a meniscus.

FIG. 2. Four different fluid arrangements inside one tube. The shaded and the white regions indicate the non-wetting and wetting fluid respectively.

FIG. 3. The motion of the menisci at the nodes. (a) The non-wetting fluid (shaded) reaches the end of the tube (position 1) and is moved a distance δ into the neighbor tubes (position 2). (b) The wetting fluid (white) reaches the end of the tubes (position 1) and the non-wetting fluid (shaded) retreat to position 2. To conserve the volume of the fluids a proper time is recorded due to the small movement δ in (a) and (b).

FIG. 4. The displacement structure obtained from a simulation at $C_a = 4.6 \times 10^{-5}$ and $M = 1.0$. The size of the lattice is 40×60 nodes and the invading non-wetting fluid (black) displaces the defending wetting fluid (gray) from below. Notice the rough front between the fluids and the trapped cluster of defending fluid left behind.

FIG. 5. The displacement structure obtained by a simulation in the regime of viscous fingering on a lattice of 60×80 nodes. $C_a = 4.6 \times 10^{-3}$ and $M = 1.0 \times 10^{-3}$. The invading, non-wetting fluid (black) displaces the defending, wetting fluid (gray) from below.

FIG. 6. ΔP (a) and P_{cg} (b) plotted as a function of time. $C_a = 4.6 \times 10^{-3}$ and $M = 1.0 \times 10^{-3}$.

FIG. 7. P_{cf} (a), and P_{cg} (b), at four different capillary numbers for the simulations with $M = 1.0 \times 10^{-3}$ at lattice size 25×35 nodes. The pressures are normalized using the average threshold pressure of the tubes. Note that P_{cg} has been subtracted by 1000 dyn/cm^2 before it was normalized to avoid overlap between the two curves at low capillary numbers.

FIG. 8. P_{cg} (a) and the capillary pressure of the meniscus traveling with the highest velocity (b) at $C_a = 1.1 \times 10^{-2}$ and $M = 1.0 \times 10^{-3}$ in the time interval between 7.0 and 12.0 s.

FIG. 9. The displacement structure obtained of a simulation in the regime of stable displacement on a lattice of 60×60 nodes. $C_a = 4.6 \times 10^{-3}$ and $M = 1.0 \times 10^2$. The invading, non-wetting fluid (black) displaces the defending, wetting fluid (gray) from below.

FIG. 10. ΔP (a), P_{cg} (b) and A_0/A (c) as functions of time for the simulations with $M = 1.0 \times 10^2$ at lattice size 60×60 (to the left) and 40×40 nodes (to the right). The vertical dashed lines indicate the saturation time where the front stabilize.

FIG. 11. ΔP (a), P_{cg} (b) and A_0/A (c) as functions of time for the five simulations with $M = 1.0 \times 10^2$ at lattice size 25×35 nodes. Note that for $C_a = 4.2 \times 10^{-3}$, 2.2×10^{-3} and 7.5×10^{-4} P_{cg} has been subtracted by 1000 dyn/cm^2 to avoid overlap of the curves. The vertical dashed lines indicate the saturation time where the front stabilize.

FIG. 12. The average front position as a function of time at $C_a = 4.6 \times 10^{-3}$ and $M = 1.0 \times 10^2$ for the lattice of 60×60 nodes.

FIG. 13. ΔP (a) and P_{cg} (b) for six simulations with $M = 1.0$ each at one of the capillary number listed in Table III. The dashed line indicates the saturation time t_s when the front has reached the saturation width w_s . Note that P_{cg} has been subtracted by 1000 dyn/cm^2 to avoid the curves from overlapping at low capillary numbers.

FIG. 14. The normalized difference $\Delta P - P_{cg}$ subtracted by 1 at $C_a = 2.3 \times 10^{-3}$ and $M = 1.0$.

TABLE I. The lattice size and the values for the injection rate and the capillary number when $M = 1.0 \times 10^{-3}$.

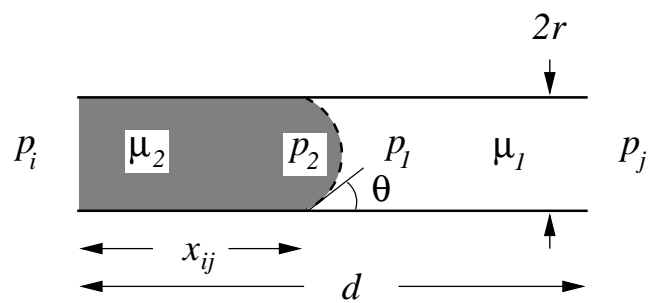
Size (nodes)	Injection rate (cm^3/min)	C_a
60×80	1.5	4.6×10^{-3}
25×35	1.4	1.1×10^{-2}
25×35	0.98	7.1×10^{-3}
25×35	0.62	4.7×10^{-3}
25×35	0.50	3.6×10^{-3}
25×35	0.099	7.2×10^{-4}
25×35	0.049	3.5×10^{-4}

TABLE II. The lattice size and the values for the injection rate and the capillary number when $M = 1.0 \times 10^2$.

Size (nodes)	Injection rate (cm^3/min)	C_a
60×60	1.5	4.6×10^{-3}
40×40	1.0	4.6×10^{-3}
25×35	2.5	1.8×10^{-2}
25×35	1.3	9.5×10^{-3}
25×35	0.57	4.2×10^{-3}
25×35	0.29	2.2×10^{-3}
25×35	0.10	7.5×10^{-4}

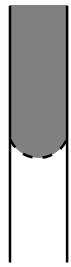
TABLE III. The values for the injection rate and the capillary number when $M = 1.0$. The lattice is 40×60 nodes.

Runs	Injection rate (cm^3/min)	C_a
3	10	2.3×10^{-3}
3	4.0	9.2×10^{-4}
3	2.0	4.6×10^{-4}
3	1.0	2.3×10^{-4}
3	0.40	9.2×10^{-5}
2	0.20	4.6×10^{-5}





(a)



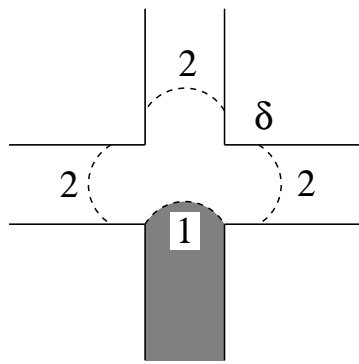
(b)



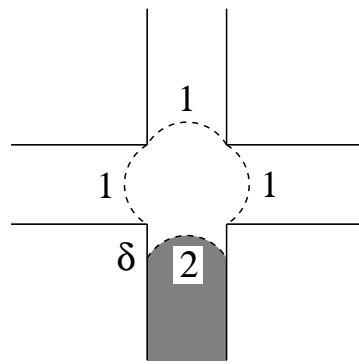
(c)



(d)



(a)



(b)

